

# DF<sup>2</sup>AM: Dual-level Feature Fusion and Affinity Modeling for RGB-Infrared Cross-modality Person Re-identification

Junhui Yin, Zhanyu Ma\*, Jiyang Xie, Shibo Nie, Kongming Liang, and Jun Guo

## Abstract

RGB-infrared person re-identification is a challenging task due to the intra-class variations and cross-modality discrepancy. Existing works mainly focus on learning modality-shared global representations by aligning image styles or feature distributions across modalities, while local feature from body part and relationships between person images are largely neglected. In this paper, we propose a Dual-level (i.e., local and global) Feature Fusion (DF<sup>2</sup>) module by learning attention for discriminative feature from local to global manner. In particular, the attention for a local feature is determined locally, i.e., applying a learned transformation function on itself. Meanwhile, to further mining the relationships between global features from person images, we propose an Affinities Modeling (AM) module to obtain the optimal intra- and inter-modality image matching. Specifically, AM employs intra-class compactness and inter-class separability in the sample similarities as supervised information to model the affinities between intra- and inter-modality samples. Experimental results show that our proposed method outperforms state-of-the-arts by large margins on two widely used cross-modality re-ID datasets SYSU-MM01 and RegDB, respectively.

## 1. Introduction

Person re-identification (re-ID) is a cross-camera image retrieval task, which aims to match persons of a given query from an image gallery collected from disjoint cameras. Many studies resort to deep metric learning [11, 48], or use classification losses as the proxy targets to extract discriminative features [17, 25, 26, 36]. With recent progress in the generative adversarial networks (GANs), another possibility is explore GANs as a style transformer to augment training data and improve the discriminative capacity of model [49, 7, 18, 22, 47].

Existing re-ID methods mainly treat visible images as single-modality and degrade dramatically in real complex scenarios where person images are captured from both dark and bright lighting environments. However, visible light cameras can not work at night. Fortunately, some surveil-

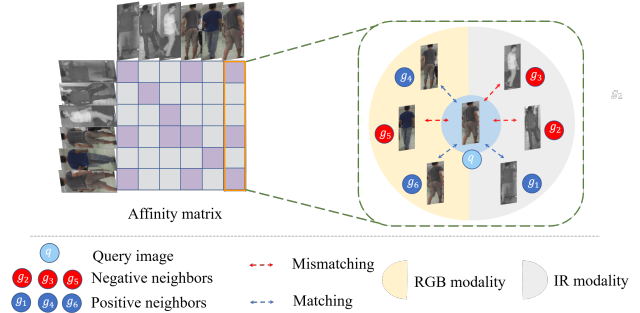


Figure 1: Affinity modeling (AM) infers cross-modality sample similarities by exploiting intra-class compactness and inter-class separability in the sample similarities. In training batch, each training image can be considered as query image and it treats all the training samples as its neighbours, where each image accepts the structure information from all the neighbours.

lance devices like infrared cameras can capture the appearance characteristics of a person under poor illumination conditions to overcome these difficulties. This yields popular research interest on RGB-IR cross-modality matching, which is more challenge due to the large discrepancy between two modalities compared with the RGB single modality. For instance, RGB images contain some discriminative cues like colors while these information are missing in infrared images.

Recently, many studies resort to two typical approaches to address the aforementioned challenges in cross-modality re-ID. The first approaches [34, 40, 43] attempt to reduce the cross-modality discrepancy with feature-level constraints like aligning feature distribution of images. The other approaches [29, 32, 30] are at input-level using GANs to transfer images from one modality to another while preserving the identity information as much as possible. The two approaches mainly focus on reducing discrepancy across modalities, whereas there is still the challenge of appearance variations in a single RGB or IR modality, including background clutter, viewpoint variations, occlusion, etc.

To address the above problem, we propose to learn attention for discriminative feature from local to global man-

ner. The critical idea behind it lies in different parts of a person containing different discriminative information. The network model can still capture useful information from the upper body using attention mechanism, regardless of a pedestrian’s lower body occluded by something (*e.g.*, a bicycle). Specifically, we propose a *local attention*: the attention for a local feature is determined locally, *i.e.*, applying a learned transformation function on itself, where the refined part-aggregated features consider the importance between different body parts. However, such local strategies do not fully exploit the feature information from a global view. Our solution is to use the global feature information from feature maps using global average pooling (GAP), which is named *global attention*. In this way, we consider both the global feature and its part information to determine importance between different body parts of a person from global and local views. This is also consistent with the perception of human in finding discriminative cues: making a comparison and then determine the importance.

The aforementioned method processes each sample independently, ignoring the relationships between person images. Thus, we present a novel and efficient similarity inference to obtain the optimal intra- and inter-modality image matching. It utilizes intra-class compactness and inter-class separability in the sample similarities as supervised information to model the affinities between intra- and inter-modality samples. In particular, every sample contains some structural information and propagates the information to its neighbors using the pairwise relations, which is shown in Figure 1. This neighbor reasoning scheme can compensate for the lack of specific information existing in the same person’s different images and further enhance the robustness of the learned feature from object-level.

In our proposed method, contextual information for RGB-IR cross-modality re-ID consists of dual levels. The lowest is the patch-level where the appearance variation (*e.g.*, data occlusion problem) is mitigated with a weighted sum over important body parts to assist more accurate information of object (*i.e.*, person). At the object level, co-existence of objects provides strong hints on identification of the same person. Experimental results show that our proposed method can surpass state-of-the-arts by large margins on two widely used cross-modality re-ID datasets SYSU-MM01 [34] and RegDB [21], respectively.

In summary, the contributions of our work include:

- We propose to learn the attention for discriminative representation by taking both local and global views of features.
- We design an efficient mutual neighbor reasoning to capture long-range dependency of objects, by modeling affinity between intra- and inter-modality images.
- Our proposed method achieves significant performance improvement over the state-of-the-arts on on the two most

popular benchmark datasets.

## 2. Related Work

### RGB-RGB single-modality person re-Identification.

Conventional person re-ID research is a RGB-RGB single modality re-ID to address the problem of matching pedestrian across non-overlapping cameras. The challenge of re-ID lies in how to learn discriminative features from person images where there are the large intra-class and small inter-class variations caused by diversity of poses, illumination conditions, viewpoint occlusion, etc. To address the aforementioned challenges, many deep re-ID methods [8, 24, 25, 19] have been proposed. Some of them resort to a partial feature learning [8, 24] and focus on the powerful network structures to align the body parts [25, 19]. Other methods try to discard the appearance variant out in metric space using loss functions, which contains contrastive loss [11], triplet loss [11], quadruplet loss [2]. Recent graph-based methods [23, 35] consider connections between sample pairs. However, these methods are developed for single-modality re-ID but not for the cross-modality re-ID due to the large discrepancy across modalities.

### RGB-IR cross-modality person re-Identification.

The large discrepancy of cross-modality re-ID comes not only from appearance variations but also from cross-modality variation between RGB and IR images. Existing studies for cross-modality re-ID can be mainly summarized into two categories of methods. The first category [34, 40, 43] attempts to align the feature distribution of training images in representation space. The work [34] focus on how to design one-stream networks such as a deep zero-padding network for evolving domain-specific nodes. The two-stream network with modality-specific [40] and top-ranking loss [43] are developed to learn multi-modality representations. In [4], a generative adversarial training method is proposed to jointly discriminate the identity and modality. [9] design a hyper-sphere manifold embedding model to learn discriminative representations from different modalities. The second approach instead uses cross-modality generative adversarial network (GAN) to transfer person images style from one modality to another. [14] collects a new ThermalWorld dataset and propose a ThermalGAN framework for color-to-thermal image translation. [32] further considers dual-level discrepancy and use a bi-directional cycle GAN [50] to generate unlabeled images as data augmentation. A hierarchical disentanglement method [3] is proposed to disentangle ID-discriminative factors and ID-excluded factors simultaneously by using pose- and illumination-invariant features from cross-modality images.

**Attention mechanisms.** Humans does not attempt to process a whole scene of the data at once. Instead, they selectively use an salient part information to make a decision [13, 20]. The above process is called attention mech-

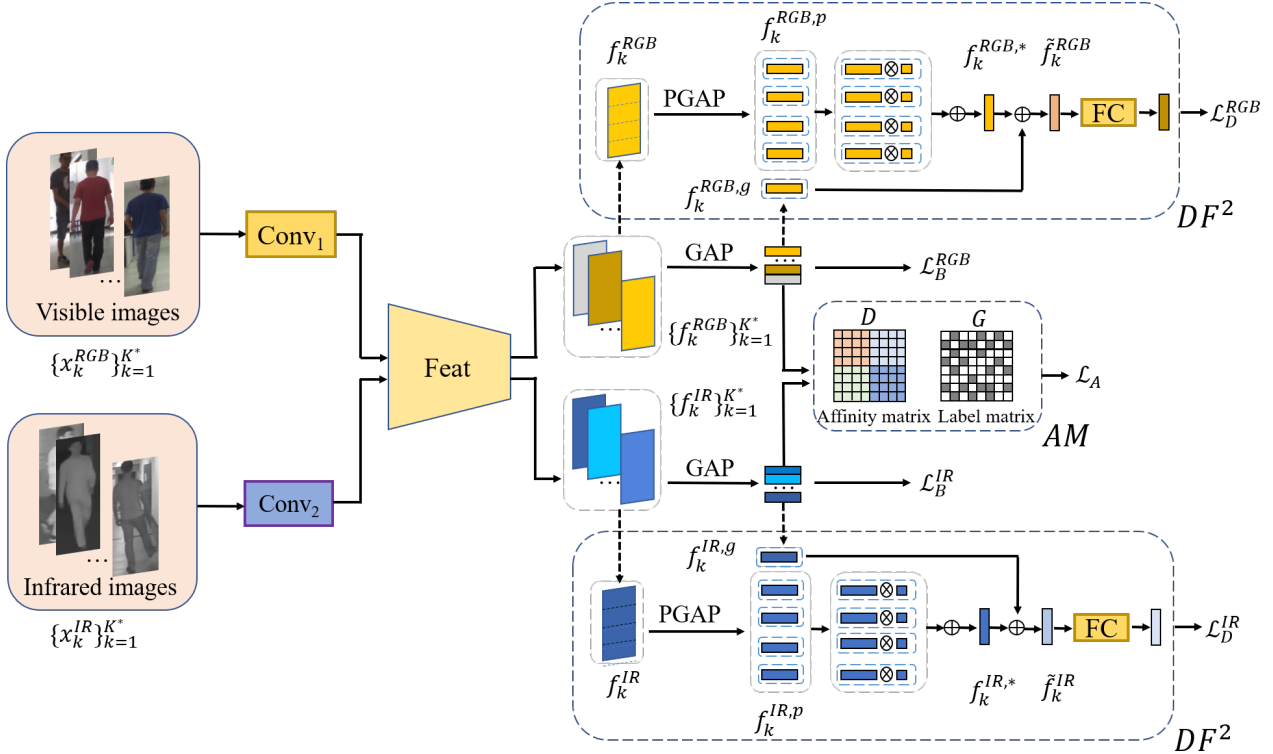


Figure 2: The architecture of our  $DF^2AM$  method. The entire framework includes two important components: the weighted-part and global feature fusion and affinities modeling for intra- and inter-modality feature matching. Our goal is to learn discriminative features and enhance the robustness of the learned features from patch-level to object-level.

anism and is actively used in many tasks including image captioning [38, 1], transfer learning [44], object localization [45]. Furthermore, the self-attention mechanism [27] is proposed to draw global dependencies of inputs. Recently, various methods [28, 31, 12, 33] use the self-attention mechanism to improve the performance of the classification model. For person re-ID, attention is used to capture spatial and temporal characteristics of pedestrian sequences from different video frames [37, 16, 16]. However, the application of these methods is limited for the cross-modality re-ID due to the different camera environments and large visual appearances change. In this work, we use attention mechanism to focus on important local features instead of processing all the data equally for cross-modality re-ID.

### 3. Methodology

In this section, we describe details of the proposed  $DF^2AM$  approach for cross-modality re-ID. We first revisit the baseline single-modality model and introduce a more efficient way for intra- and inter-modality feature matching. Then, the details of the proposed  $DF^2AM$ , founded on the above finding, are presented for learning discriminative features, and enhancing the robustness of the learned feature

from patch-level to object-level.

#### 3.1. Single-modality Person Re-identification Re-visit

We first present the baseline single-modality re-ID model, which offers a promising way to learn discriminative global features. The training process can be treated as a conventional classification problem [46]. To learn the feature embedding, the baseline usually learn the parameters with manual annotations where extracted feature  $f_k, k = 1, \dots, K$  is associated with a one-hot label  $y_k$ . The classification procedure is achieved by minimizing a cross-entropy loss  $\mathcal{L}_{ID}$ . Meanwhile, hard-mining triplet loss  $\mathcal{L}_{BH}$  [11] is used to optimize the triplet-wise relationships among different person images. Thus, the baseline re-ID model is optimized by minimizing the following loss function as

$$\mathcal{L}_B = \mathcal{L}_{ID} + \mathcal{L}_{BH}, \quad (1)$$

where

$$L_{ID} = -\frac{1}{K} \sum_{i=1}^K \log p(y_k | f_k), \quad (2)$$

$$L_{BH} = \sum_{i=1}^N \sum_{a=1}^M \left[ m + \overbrace{\max_{p=1, \dots, M} d(f_a, f_p)}^{\text{hardest positive}} - \underbrace{\max_{\substack{j=1, \dots, N \\ n=1, \dots, M \\ j \neq i}} d(f_a, f_n)}_{\text{hardest negative}} \right]_+, \quad (3)$$

Here,  $d$  is a metric function (*i.e.*, European distance) measuring distances in the embedding space,  $K = MN$  is the number of images in single modality,  $N$  is randomly selected identity number, and  $M$  is randomly sampled image number of each identity.  $p(y_i | f_k)$  is the predicted probability that the encoded feature  $f_k$  belongs to its identity  $y_k$ , which is obtained by a classifier.

### 3.2. The overall framework

To explore richer visual patterns for cross-modality re-ID, we propose DF<sup>2</sup>AM method and integrate it with a conventional re-ID network. The DF<sup>2</sup>AM is fulfilled from the perspective of patch-level and object-level, and is deployed as dual-level feature fusion and affinity modeling modules. The learning procedure is fulfilled by optimizing a joint objective function, as

$$\mathcal{L}_{Final} = \mathcal{L}_B + \lambda \mathcal{L}_D + \zeta \mathcal{L}_A, \quad (4)$$

where  $\mathcal{L}_B = \mathcal{L}_B^{RGB} + \mathcal{L}_B^{IR}$ . Here,  $\mathcal{L}_B^{RGB}$  and  $\mathcal{L}_B^{IR}$  are the baseline loss for RGB and IR modality respectively,  $\mathcal{L}_D$  denotes the classification loss for dual-level feature fusion module, and  $\mathcal{L}_A$  is the affinity modeling loss.  $\lambda$  and  $\zeta$  are the regularization factors.

As shown in Figure 2, we first feed visible image batch  $X^{RGB} = \{x_k^{RGB}\}_{k=1}^{K^*}$  and infrared image batch  $X^{IR} = \{x_k^{IR}\}_{k=1}^{K^*}$  into different convolutional layers to capture modality-specific low-level feature patterns, where  $2K^*$  is the batch size. Then, we use the shared feature extractor (*i.e.*, convolutional layers)  $Feat$  to transform the specific features onto a common representation space to acquire modality-sharable high-level features, formulated as

$$f_k^{RGB} = Feat(Conv_1(x_k^{RGB})),$$

$$f_k^{IR} = Feat(Conv_2(x_k^{IR})).$$

Here,  $f_k^{RGB} \subseteq \mathbb{R}^{C \times H \times W}$  and  $f_k^{IR} \subseteq \mathbb{R}^{C \times H \times W}$  for visible and infrared images, respectively. Note that  $C$  is the number of channels,  $H$  and  $W$  are height and width, respectively. With the obtained high-level features, intra- and inter-modality feature learning are required to be undertaken. For the intra-modality feature learning, dual-level feature fusion (DF<sup>2</sup>) module learns part-aggregated feature embeddings, and combine them with global features

to enhance the representative capacity of features for intra-modality re-ID. Meanwhile, the shared feature extractor is to learn aligned features for bridging RGB and IR modalities. For inter-modality feature matching, a similarity inference is presented to model the affinities between both intra- and inter-modality global features. This neighbor reasoning scheme utilizes intra-class compactness and inter-class separability in the sample similarities to enhance the robustness of the learned feature from object-level.

### 3.3. Dual-level Feature Fusion

Previous cross-modality re-ID models [9, 30] commonly focus on constructing feature- or image-level constraints for reducing distribution discrepancy in same identities. However, the challenge of appearance variations, including background clutter, viewpoint variations, and occlusion, are not overcome by only using the global features. In this case, we propose the local attention mechanism, which refines part-aggregated features by a learned transformation function on itself, to consider the importance between different body parts of a person.

We take the feature  $f_k^{RGB}$  from the RGB modality as an example. In our local attention mechanism, a patch-wise average pooling (PAP) is used to extract  $P$  local features  $f_k^{RGB,p} \subseteq \mathbb{R}^C$ ,  $p = 1, \dots, P$  (assuming  $P$  is a factor of  $H$ ) by

$$f_k^{RGB,p} = \frac{P}{WH} \sum_{w=1}^W \sum_{h=\frac{(p-1)H}{P}+1}^{\frac{pH}{P}} f_{k,:,h,w}^{RGB}, \quad (5)$$

where PAP first splits the feature maps  $f_k^{RGB}$  into  $P$  horizontal feature spatial parts and then generates local features  $f_k^{RGB,p}$  by compressing spatial parts using global average pooling (GAP).

To obtain a discriminative part-aggregated feature  $\tilde{f}_k^{RGB}$ , we compute a weighted summation of local features from body parts together with learnable local attention as weight  $\omega = (\omega_1, \dots, \omega_P)^T$ . In summary, it is formulated by

$$f_k^{RGB,*} = \sum_{p=1}^P \tilde{\omega}_p f_k^{RGB,p}, \quad (6)$$

where  $\tilde{\omega}_p = \frac{e^{\omega_p}}{\sum_{p'=1}^P e^{\omega_{p'}}$ .

Although the aforementioned local attention mechanism assigns weights for local features, such local strategy cannot fully exploit the feature information from a global view and affect the representative capacity of feature, which is discussed in the experiments. Thus, we combine global feature with local feature as

$$\tilde{f}_k^{RGB} = \text{BN}(f_k^{RGB,g}) + f_k^{RGB,*}, \quad (7)$$

where  $\text{BN}(\cdot)$  is batch normalization and  $f_k^{RGB,g}$  represents the GAP output of the input feature map  $f_k^{RGB}$ . For the in-

frared modality, we can also obtain the discriminative representation  $\tilde{f}_k^{\text{IR}}$  by using  $f_k^{\text{IR}}$  in the same way. Finally, the loss for  $DF^2$  can be expressed by

$$\begin{aligned} \mathcal{L}_D &= \mathcal{L}_D^{\text{RGB}} + \mathcal{L}_D^{\text{IR}} \\ &= -\frac{1}{K^{\text{RGB}}} \sum_{k=1}^{K^{\text{RGB}}} \log p(y_k | \tilde{f}_k^{\text{RGB}}) \\ &\quad - \frac{1}{K^{\text{IR}}} \sum_{k=1}^{K^{\text{IR}}} \log p(y_k | \tilde{f}_k^{\text{IR}}), \end{aligned} \quad (8)$$

where  $K^{\text{RGB}}$  ( $K^{\text{IR}}$ ) is the number of images in visible (infrared) modality, and each of features  $\tilde{f}_k^{\text{RGB}}$  and  $\tilde{f}_k^{\text{IR}}$  corresponds to an identity label  $y_k \in \{1, \dots, N\}$ .

### 3.4. Affinity Modeling

A common strategy to align feature distribution of images is utilizing hard-mining triplet loss [11]. For each chosen anchor, it is required for selecting the hard positive/negative exemplars from within a mini-batch. The above strategy is complex and required for additional computing resources. To better align feature distribution of images across intra- and inter-modality, we propose a simple and efficient similarity inference to obtain the optimal intra- and inter-modality image matching. It utilizes intra-class compactness and inter-class separability in the sample similarities as supervised information to model the affinities between intra- and inter-modality samples. Here we aim to ensure that an image of a specific person is closer to all positive images of the same person than any (negative) image of any other person. In addition, our method is simple and efficient since no hard pairs are mined and all the pairs are utilized in training.

**Affinity matrix construction.** We first use the encoded global features  $f_k^{\text{RGB,g}}$  and  $f_k^{\text{IR,g}}$  from two modalities to model the pair-wise affinities (affinity matrix  $D$ ), which is defined as

$$D = \begin{pmatrix} D_{\text{RGB,RGB}} & D_{\text{RGB,IR}} \\ D_{\text{IR,RGB}} & D_{\text{IR,IR}} \end{pmatrix}, \quad (9)$$

where  $D_{\text{RGB,RGB}}$  and  $D_{\text{IR,IR}}$  are intra-modality affinity matrices of the visible and infrared modalities, respectively, and  $D_{\text{RGB,IR}}$  and  $D_{\text{IR,RGB}}$  are inter-modality affinity matrices. At each training step, an identity-balanced sampling strategy are adopted for training [42]. For each of  $N^*$  different randomly selected identities,  $M^*$  visible and  $M^*$  infrared images are randomly sampled, resulting in batch size  $2K^*$  is equal to  $2N^*M^*$  and  $D_{a,b}$ ,  $a, b \in \{\text{RGB, IR}\}$  are  $K^* \times K^*$ -dimensional. The elements of the sub-matrices  $D_{a,b}$ ,  $a, b \in \{\text{RGB, IR}\}$  are calculated by

$$D_{a,b}^{ij} = \left\| \frac{f_i^{a,g}}{\|f_i^{a,g}\|_2} - \frac{f_j^{b,g}}{\|f_j^{b,g}\|_2} \right\|_2 \in [0, +\infty), \quad (10)$$

where  $\|\cdot\|_2$  is  $L_2$ -norm. It is noted that other distance metrics, such as cosine similarity, can be also used. In this work, we adopt the Euclidean distance between normalized global features and smaller distance value means more similar.

**Ground truth affinity matrix.** According to label information of each image, we construct a ground truth affinity, which corresponds to the affinity matrix and performs as the ground truth labels of the similarity inference. The label matrix is defined as a binary matrix  $G = [G^{ij}]$ ,  $i, j = 1, \dots, 2K^*$ , where  $G^{ij} = 1$  if the  $i^{\text{th}}$  and the  $j^{\text{th}}$  samples belong to one same identity, otherwise zero.

Thus, our aim is that the affinity elements of negative pairs are as close to one as possible and that of positive pairs are as close to zero as possible. This can be achieved by minimizing the following mean  $L_1$  error between affinity matrix and its ground truth,

$$\mathcal{L}_1 = \|D - (\mathbb{1} - G) \cdot \delta\|_1 \rightarrow 0, \quad (11)$$

where  $\mathbb{1}$  is a matrix whose elements are all 1 and  $\delta$  is a suitable large value.

Theoretically, the above consistency condition is a necessary but not sufficient requirement for discriminative embeddings. This may in practice induce model converge to bad local minima early in training, which is also proved by our experiment. The main reason is all the positive and negative pairs are still treated equally when some pairs' distances are suitable enough. To address this, our solution is to relax the learning objective. We expect the affinity elements of negative pairs are larger than that of positive pairs, which can be achieved by constraining a suitable margin  $m$  between the distances of positive and negative pairs. Thus, we modify the objective loss function to

$$\mathcal{L}_A = \sum_{i=1}^{2K^*} \sum_{j=1}^{2K^*} [D^{ij} \otimes G^{ij} - (D^{ij} - m) \otimes (1 - G^{ij})]_+, \quad (12)$$

where  $m$  is a margin and  $\otimes$  presents Hadamard product.

This loss makes sure that the affinity elements of negative pairs are large at least a margin  $m$ . The advantage of this formulation is that, compared with hard-mining triplet loss [11], we can easily optimize this loss over the whole dataset without a long enough training and all points of the same class merely need to be closer to each other than to any point from a different class.

## 4. Experimental Results

### 4.1. Datasets and Settings

**Datasets.** The proposed method is evaluated over two widely used cross-modality datasets, SYSU-MM01 [34] and RegDB [21]. SYSU-MM01 is a popular RGB-IR re-ID dataset, which contains images of 419 identities cap-

Setting	All Search				Indoor Search			
	Method	r = 1	r = 10	r = 20	mAP	r = 1	r = 10	r = 20
One-stream [34](ICCV'17)	12.04	49.68	66.74	13.67	16.94	63.55	82.10	22.95
Two-stream [34](ICCV'17)	11.65	47.99	65.50	12.85	15.60	61.18	81.02	21.49
Zero-Pad [34](ICCV'17)	14.80	54.12	71.33	15.95	20.58	68.38	85.79	26.92
TONE [40](AAAI'18)	12.52	50.72	68.60	14.42	20.82	68.36	84.46	26.38
HCML [40](AAAI'18)	14.32	53.16	69.17	16.16	24.52	73.25	86.73	30.08
cmGAN [4](IJCAI'18)	26.97	67.51	80.56	31.49	31.63	77.23	89.18	42.19
BDTR [41](TIFS'19)	27.32	66.96	81.07	27.32	31.92	77.18	89.28	41.86
eBDTR [9](AAAI'19)	27.82	67.34	81.34	28.42	32.46	77.42	89.62	42.46
HSME [9](AAAI'19)	20.68	32.74	77.95	23.12	-	-	-	-
D <sup>2</sup> RL [32](CVPR'19)	28.90	70.60	82.40	29.20	-	-	-	-
MAC [39](TIP'20)	33.26	79.04	90.09	36.22	36.43	62.36	71.63	37.03
MSR [6](TIP'19)	37.35	83.40	93.34	38.11	39.64	89.29	97.66	50.88
AlignGAN [29](ICCV'19)	42.40	85.00	93.70	40.70	45.90	87.60	94.40	54.30
Xmodal [15](AAAI'20)	49.92	89.79	95.96	50.73	-	-	-	-
DDAG [42](ECCV'20)	54.75	90.39	95.81	53.02	61.20	94.06	98.41	67.98
Ours	<b>56.93</b>	<b>90.80</b>	<b>96.11</b>	<b>55.10</b>	<b>66.39</b>	<b>94.93</b>	<b>98.55</b>	<b>71.52</b>

Table 1: Experimental results of the proposed DF<sup>2</sup>AM and state-of-the-art methods on on SYSU-MM01 dataset under two different settings. Rank at r accuracy (%) and mAP (%) are reported.

tured in both indoor and outdoor environments. The training set includes 22,258 RGB images and 11,909 IR images of 395 persons, and the testing set contains 96 identities, with 3,803 IR images for the query and 301 RGB images for the gallery set. There are two different testing settings for RGB-IR re-ID: indoor-search and all-search [34]. All-search mode treats images from all RGB cameras as the gallery set, while the images of gallery set are captured by two indoor RGB cameras in the indoor-search mode. RegDB contains 412 persons and 8,240 images, where each person has 10 RGB images and 10 IR images. There are 4,120 images of 206 persons for training and the remaining images of 206 persons for testing. The testing set has two evaluation modes, Visible to Infrared and Infrared to Visible, where the former is to search RGB images from a infrared image and the latter is to search IR images from a Visible image. The stable result is obtained over 500 repetitions on a random split.

**Evaluation protocols.** We use two standard evaluation protocols as evaluation metrics: Cumulative Matching Characteristic (CMC) and mean average precision (mAP). The Rank- $k$  identification rate in the CMC curve represents the cumulative rate of true matches in the top- $k$  position, while mAP treats person re-identification as a retrieval task.

**Implementation details.** We adopt ResNet-50 [10] with the last classification layer removed as the backbone network and initialize it by using parameters pre-trained on ImageNet [5]. We randomly sample  $N^*$  identities, and then randomly sample  $M^*$  visible and  $M^*$  infrared images to

constitute a training batch, so that the mini-batch size is  $2K^* = 2N^* \times M^*$ . In this paper,  $N^*$  and  $M^*$  are set to 8 and 4, respectively. We resize input images to  $256 \times 128$  and then employ random cropping and flipping as data augmentation for them. During training, we also use the SGD optimizer with the momentum parameter 0.9 and the initial learning rate 0.1 for 80 epoches. The learning rate decays by 0.1 and 0.01 at the 30th and 50th epoch, respectively.

#### 4.2. Comparisons with SOTA in Cross-Modality Person Re-ID

In this section, we compare the proposed method with a number of cross-modality re-ID methods, including One-stream [34], Two-stream [34], Zero-Pad [34], TONE [40], HCML [40], cmGAN [4], BDTR [41], BDTR [41], HSME [9], D2RL [32], MAC [39], MSR [6], AlignGAN [29], Xmodal [15], and DDAG [42]. Table 1 and 2 summary the experimental results on the SYSU-MM01 and the RegDB datasets, respectively.

Table 1 reports the experimental results on SYSU-MM01. Our proposed method achieves better overall performance than all the other methods in terms of all the evaluation metrics. Specifically, in all-search mode, our method can obtain 56.93% for Rank-1 and 55.10% for mAP in the all-search mode, which surpass the second best approach (*i.e.*, DDAG [42]) by 2.18% and 2.08%, respectively. Similar results are observed in indoor-search mode. Compared to the current SOTA method, we achieve 5.19 points and 3.54 points improvement on Rank-1 and mAP,

Setting	Visible to Infrared				Infrared to Visible			
	Method	r = 1	r = 10	r = 20	mAP	r = 1	r = 10	r = 20
HCML [40](AAAI'18)	24.44	47.53	56.78	20.08	21.70	45.02	55.58	22.24
Zero-Pad [34](ICCV'17)	17.75	34.21	44.35	18.90	16.63	34.68	44.25	17.82
BDTR [41](TIFS'19)	33.56	58.61	67.43	32.76	32.92	58.46	68.43	31.96
eBDTR [41](AAAI'19)	34.62	58.96	68.72	33.46	34.21	58.74	68.64	32.49
HSME [9](AAAI'19)	50.85	73.36	81.66	47.00	50.15	72.40	81.07	46.16
D <sup>2</sup> RL [32](CVPR'19)	43.4	66.1	76.3	44.1	-	-	-	-
MAC [39](TIP'20)	36.43	62.36	71.63	37.03	36.20	61.68	70.99	36.63
MSR [6](TIP'19)	48.43	70.32	79.95	48.67	-	-	-	-
AlignGAN [29](ICCV'19)	57.90	-	-	53.60	56.30	-	-	53.40
Xmodal [15](AAAI'20)	62.21	83.13	91.72	60.18	-	-	-	-
DDAG [42](ECCV'20)	69.34	86.19	91.49	63.46	68.06	85.15	90.31	61.80
Ours	<b>73.06</b>	<b>87.96</b>	<b>91.51</b>	<b>67.81</b>	<b>70.49</b>	<b>85.78</b>	<b>90.44</b>	<b>63.85</b>

Table 2: Performance comparison with the existing methods on RegDB dataset under visible- infrared and infrared-visible settings. Rank at r accuracy (%) and mAP (%) are reported.

respectively. The above impressive performance suggests that our method can learn better modality-sharable features from patch-level to object-level.

We also evaluate our method against existing competing approaches on RegDB in Table 2. As shown in Table 2, Our method always outperforms others by large margins in different query settings. For the Visible to Infrared mode, it reaches 73.06% on Rank-1 and 67.81% on mAP, 3.72% and 4.35% higher than the current SOTA (DDGA), respectively. For Infrared to Visible, the improvements are 2.43% on rank-1 and 2.05% on mAP. This indicates that our DF<sup>2</sup>AM is robust to different evaluation modes.

### 4.3. Ablation Study

Extensive experiments are conducted under four different settings in Table 3 to evaluate each component of our proposed method: (1) The effectiveness of DF<sup>2</sup> module, (2) The effectiveness of AM module, (3) The necessity of taking Baseline into our method. All the experiments are conducted on SYSU-MM01 dataset with two evaluation modes.

As shown in Table 3, single-modality re-ID model obtain a better result than current some method. This indicates that some training tricks taken from single-modality Re-ID [67] also contributes to the performance of our method. Next, we directly merge DF<sup>2</sup> into the training process based on baseline model, which improves mAP scores by 2.76% and 3.31% for both evaluation modes. The above impressive improvements demonstrate that learning dual-level features is beneficial for cross-modality Re-ID. Similar results can be observed when AM is integrated into the training process, which also demonstrates the effectiveness of AM module. As the fifth line of Table 3 shows, the performance is further improved when we aggregate two modules with

Settings	All Search		Indoor Search	
	Baseline	DF <sup>2</sup>	AM	DF <sup>2</sup> AM
Baseline	✓			
DF <sup>2</sup>	✓	✓		
AM			✓	
DF <sup>2</sup> AM	✓	✓	✓	✓

Table 3: Ablation study. We evaluate five settings on SYSU-MM01 dataset. “Baseline”, “Baseline” with DF<sup>2</sup>, “Baseline” with AM, DF<sup>2</sup> with AM, and our DF<sup>2</sup>AM. Our method achieves the best result among other competitors.

Method	mAP	r=1	r=5	r=10
DF <sup>2</sup> AM(3 parts)	68.06	62.45	91.71	96.83
DF <sup>2</sup> AM(4 parts)	<b>71.52</b>	<b>66.39</b>	<b>94.93</b>	<b>98.55</b>
DF <sup>2</sup> AM(5 parts)	70.40	65.17	92.93	97.69

Table 4: The performance of proposed DF<sup>2</sup>AM with different number of splitted feature parts when trained on SYSU-MM01 dataset and tested on indoor search mode.

baseline. The impressive improvement suggests that these components are mutually beneficial to each other. However, without baseline, the performance of our method has a slight decline, demonstrating the necessity of taking Baseline into our method.

In addition, we compare the performance of DF<sup>2</sup>AM with different number of sliced horizontal feature parts. As shown in Table 4, our method achieves the best results when the feature maps are splitted into four parts. In this way, lo-

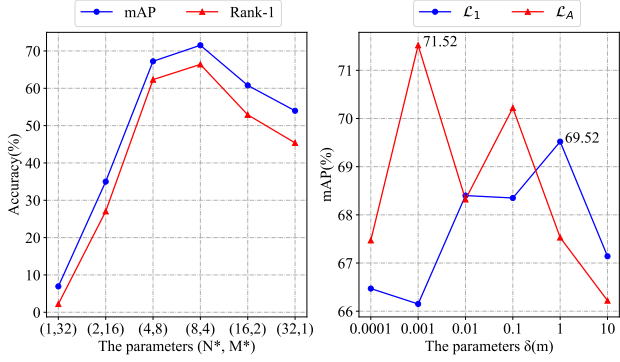


Figure 3: The experimental results on SYSU-MM01 under indoor-search mode. Left: The performance along with different parameters  $(N, M)$ . Right: The performance of our method with different loss functions under varying values of parameters  $\delta(m)$ .

cal features contain the most discriminative information for cross-modality re-ID.

**How do the identity and sample numbers of sampling strategy affect representation quality?** The hyper-parameter  $N^*$  and  $M^*$  controls identity number and sample numbers for each identity in training batch, respectively. For fair comparison, batch size  $2K^*$  is fixed as 64, while  $K^*$ ,  $N^*$  and  $M^*$  satisfy the condition  $K^* = M^*N^*$ . Figure 3 shows how the re-ID performance varies with different numbers of person identities,  $N^*$ . It can be observed that as  $N^*$  increases from 1 to 8, the re-ID performance continues rising, and the performance begins to decrease when  $N^*$  gets larger. That is, the best accuracy is achieved with  $N^* = 8$  and  $M^* = 4$ . The main reason is when  $N^*$  is too small, the learned similarity is not adequate, which makes the model difficult to match features of the same identity during affinity modeling. When  $N^*$  is too large, images of different persons will be reduced, which harms the network training for similarity inference.

**The impact of  $\mathcal{L}_A$  and  $\mathcal{L}_1$ .** As shown in Figure 3, our method (w/  $\mathcal{L}_A$ ) achieves the best performance of mAP=71.52% on SYSU-MM01, 2.00% higher than directly using  $\mathcal{L}_1$ . Such results prove the necessity and effectiveness of our affinity modeling loss  $\mathcal{L}_A$ , which alleviates the problem of model converging to local minima early in training stage. In addition, it can be observed that compared with our method (w/  $\mathcal{L}_1$ ), smaller value  $m(\delta)$  leads to the better results of our method (w/  $\mathcal{L}_A$ ) and vice versa, which is consistent with our expectation. The main reason is that our network is trained with  $\mathcal{L}_A$ , which avoids pushing always images of different identities separate as  $\mathcal{L}_1$ , but it has a relatively small strength (*i.e.*,  $m$ ) to force them separate.

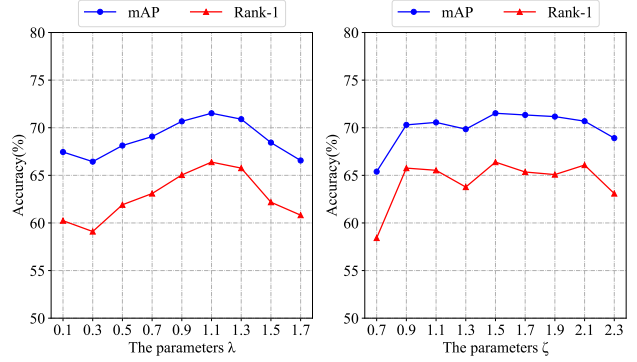


Figure 4: Performance evaluation of our proposed method with different values of  $\lambda$  and  $\zeta$  on SYSU-MM01 under indoor-search mode.

#### 4.4. Parameter sensitivities

The parameter  $\lambda$  balances the effect of  $DF^2$  module and baseline model. We evaluate our method with different values for the parameter  $\lambda$  in Figure 4. As  $\lambda$  increases, the accuracy improves at first. When  $\lambda = 1.1$ , we obtain the best performance. After that, the performance begins to decline. Similar results can be observed when we vary parameter values of  $\zeta$  from 0.1 to 2.1. The optimal accuracy is achieved when  $\zeta = 1.5$ . Despite the performances vary with different parameter values, most results by our approach outperform the current state-of-the-arts significantly.

### 5. Conclusions

In this paper, we propose an efficient network that integrates feature information at different modalities into person re-identification. we introduce two key modules into the network and fuse dual-level feature to reduce the cross-modality discrepancy. The proposed  $DF^2$  module considers both the global feature and its part information to determine importance between different body parts of a person from global and local views. The AM module uses intra-class compactness and inter-class separability in the sample similarities as supervised information to model the relationships between person images. Ablation studies demonstrate the effectiveness of the proposed modules in improving the identification accuracy. Extensive experiments with our state-of-the-art results on two competitive datasets further demonstrate the effectiveness and generality of our  $DF^2AM$  approach.

### References

- [1] Long Chen, Hanwang Zhang, Jun Xiao, Liqiang Nie, Jian Shao, Wei Liu, and Tat-Seng Chua. Sca-cnn: spatial and channel-wise attention in convolutional networks for image



- captioning. In *Proceedings of the IEEE Conference on Computer Vision and Pattern Recognition*, pages 5659–5667, 2017.
- [2] Weihua Chen, Xiaotang Chen, Jianguo Zhang, and Kaiqi Huang. Beyond triplet loss: a deep quadruplet network for person re-identification. In *Proceedings of the IEEE conference on Computer Vision and Pattern Recognition*, pages 403–412, 2017.
- [3] Seokeon Choi, Sumin Lee, Youngeun Kim, Taekyung Kim, and Changick Kim. Hi-cmd: hierarchical cross-modality disentanglement for visible-infrared person re-identification. In *Proceedings of the IEEE Conference on Computer Vision and Pattern Recognition*, pages 10257–10266, 2020.
- [4] Pingyang Dai, Rongrong Ji, Haibin Wang, Qiong Wu, and Yuyu Huang. Cross-modality person re-identification with generative adversarial training. In *Proceedings of International Joint Conference on Artificial Intelligence*, volume 1, page 2, 2018.
- [5] Jia Deng, Wei Dong, Richard Socher, Li-Jia Li, Kai Li, and Li Fei-Fei. Imagenet: A large-scale hierarchical image database. In *Proceedings of the IEEE Conference on Computer Vision and Pattern Recognition*, pages 248–255. IEEE, 2009.
- [6] Zhanxiang Feng, Jianhuang Lai, and Xiaohua Xie. Learning modality-specific representations for visible-infrared person re-identification. *IEEE Transactions on Image Processing*, 29:579–590, 2019.
- [7] Yixiao Ge, Zhuowan Li, Haiyu Zhao, Guojun Yin, Shuai Yi, Xiaogang Wang, and Hongsheng Li. Fd-gan: Pose-guided feature distilling gan for robust person re-identification. *arXiv preprint arXiv:1810.02936*, 2018.
- [8] Jianyuan Guo, Yuhui Yuan, Lang Huang, Chao Zhang, Jin-Ge Yao, and Kai Han. Beyond human parts: Dual part-aligned representations for person re-identification. In *Proceedings of the IEEE International Conference on Computer Vision*, pages 3642–3651, 2019.
- [9] Yi Hao, Nannan Wang, Jie Li, and Xinbo Gao. Hsme: hypersphere manifold embedding for visible thermal person re-identification. In *Proceedings of the AAAI Conference on Artificial Intelligence*, volume 33, pages 8385–8392, 2019.
- [10] Kaiming He, Xiangyu Zhang, Shaoqing Ren, and Jian Sun. Deep residual learning for image recognition. In *Proceedings of the IEEE conference on Computer Vision and Pattern Recognition*, pages 770–778, 2016.
- [11] Alexander Hermans, Lucas Beyer, and Bastian Leibe. In defense of the triplet loss for person re-identification. *arXiv preprint arXiv:1703.07737*, 2017.
- [12] Jie Hu, Li Shen, and Gang Sun. Squeeze-and-excitation networks. In *Proceedings of the IEEE Conference on Computer Vision and Pattern Recognition*, pages 7132–7141, 2018.
- [13] Laurent Itti, Christof Koch, and Ernst Niebur. A model of saliency-based visual attention for rapid scene analysis. *IEEE Transactions on Pattern Analysis and Machine Intelligence*, 20(11):1254–1259, 1998.
- [14] Vladimir V Kniaz, Vladimir A Knyaz, Jiri Hladuvka, Walter G Kropatsch, and Vladimir Mizginov. Thermalgan: Multimodal color-to-thermal image translation for person re-identification in multispectral dataset. In *Proceedings of the European Conference on Computer Vision Workshops*, pages 0–0, 2018.
- [15] Diangang Li, Xing Wei, Xiaopeng Hong, and Yihong Gong. Infrared-visible cross-modal person re-identification with an x modality. In *Proceedings of the AAAI Conference on Artificial Intelligence*, volume 34, pages 4610–4617, 2020.
- [16] Shuang Li, Slawomir Bak, Peter Carr, and Xiaogang Wang. Diversity regularized spatiotemporal attention for video-based person re-identification. In *Proceedings of the IEEE Conference on Computer Vision and Pattern Recognition*, pages 369–378, 2018.
- [17] Wei Li, Xiatian Zhu, and Shaogang Gong. Person re-identification by deep joint learning of multi-loss classification. *arXiv preprint arXiv:1705.04724*, 2017.
- [18] Jinxian Liu, Bingbing Ni, Yichao Yan, Peng Zhou, Shuo Cheng, and Jianguo Hu. Pose transferrable person re-identification. In *Proceedings of the IEEE Conference on Computer Vision and Pattern Recognition*, pages 4099–4108, 2018.
- [19] Kan Liu, Bingpeng Ma, Wei Zhang, and Rui Huang. A spatio-temporal appearance representation for video-based pedestrian re-identification. In *Proceedings of the IEEE International Conference on Computer Vision*, pages 3810–3818, 2015.
- [20] Volodymyr Mnih, Nicolas Heess, Alex Graves, and Koray Kavukcuoglu. Recurrent models of visual attention. *arXiv preprint arXiv:1406.6247*, 2014.
- [21] Dat Tien Nguyen, Hyung Gil Hong, Ki Wan Kim, and Kang Ryoung Park. Person recognition system based on a combination of body images from visible light and thermal cameras. *Sensors*, 17(3):605, 2017.
- [22] Xuelin Qian, Yanwei Fu, Tao Xiang, Wenxuan Wang, Jie Qiu, Yang Wu, Yu-Gang Jiang, and Xiangyang Xue. Pose-normalized image generation for person re-identification. In *Proceedings of the European Conference on Computer Vision*, pages 650–667, 2018.
- [23] Yantao Shen, Hongsheng Li, Shuai Yi, Dapeng Chen, and Xiaogang Wang. Person re-identification with deep similarity-guided graph neural network. In *Proceedings of the European Conference on Computer Vision*, pages 486–504, 2018.
- [24] Yifan Sun, Qin Xu, Yali Li, Chi Zhang, Yikang Li, Shengjin Wang, and Jian Sun. Perceive where to focus: Learning visibility-aware part-level features for partial person re-identification. In *Proceedings of the IEEE Conference on Computer Vision and Pattern Recognition*, pages 393–402, 2019.
- [25] Yifan Sun, Liang Zheng, Yi Yang, Qi Tian, and Shengjin Wang. Beyond part models: Person retrieval with refined part pooling (and a strong convolutional baseline). In *Proceedings of the European Conference on Computer Vision*, pages 480–496, 2018.
- [26] Zheng Tang, Milind Naphade, Ming-Yu Liu, Xiaodong Yang, Stan Birchfield, Shuo Wang, Ratnesh Kumar, David Anastasiu, and Jenq-Neng Hwang. Cityflow: A city-scale benchmark for multi-target multi-camera vehicle tracking and re-identification. In *Proceedings of the IEEE Conference*

- on *Computer Vision and Pattern Recognition*, pages 8797–8806, 2019.
- [27] Ashish Vaswani, Noam Shazeer, Niki Parmar, Jakob Uszkoreit, Llion Jones, Aidan N Gomez, Lukasz Kaiser, and Illia Polosukhin. Attention is all you need. *arXiv preprint arXiv:1706.03762*, 2017.
- [28] Fei Wang, Mengqing Jiang, Chen Qian, Shuo Yang, Cheng Li, Honggang Zhang, Xiaogang Wang, and Xiaoou Tang. Residual attention network for image classification. In *Proceedings of the IEEE conference on Computer Vision and Pattern Recognition*, pages 3156–3164, 2017.
- [29] Guan’an Wang, Tianzhu Zhang, Jian Cheng, Si Liu, Yang Yang, and Zengguang Hou. Rgb-infrared cross-modality person re-identification via joint pixel and feature alignment. In *Proceedings of the IEEE International Conference on Computer Vision*, pages 3623–3632, 2019.
- [30] Guan-An Wang, Tianzhu Zhang, Yang Yang, Jian Cheng, Jianlong Chang, Xu Liang, and Zeng-Guang Hou. Cross-modality paired-images generation for rgb-infrared person re-identification. In *Proceedings of the AAAI Conference on Artificial Intelligence*, volume 34, pages 12144–12151, 2020.
- [31] Xiaolong Wang, Ross Girshick, Abhinav Gupta, and Kaiming He. Non-local neural networks. In *Proceedings of the IEEE Conference on Computer Vision and Pattern Recognition*, pages 7794–7803, 2018.
- [32] Zhixiang Wang, Zheng Wang, Yinqiang Zheng, Yung-Yu Chuang, and Shin’ichi Satoh. Learning to reduce dual-level discrepancy for infrared-visible person re-identification. In *Proceedings of the IEEE Conference on Computer Vision and Pattern Recognition*, pages 618–626, 2019.
- [33] Sanghyun Woo, Jongchan Park, Joon-Young Lee, and In So Kweon. Cbam: Convolutional block attention module. In *Proceedings of the European Conference on Computer Vision*, pages 3–19, 2018.
- [34] Ancong Wu, Wei-Shi Zheng, Hong-Xing Yu, Shaogang Gong, and Jianhuang Lai. Rgb-infrared cross-modality person re-identification. In *Proceedings of the IEEE International Conference on Computer Vision*, pages 5380–5389, 2017.
- [35] Jinlin Wu, Yang Yang, Hao Liu, Shengcai Liao, Zhen Lei, and Stan Z Li. Unsupervised graph association for person re-identification. In *Proceedings of the IEEE International Conference on Computer Vision*, pages 8321–8330, 2019.
- [36] Yu Wu, Yutian Lin, Xuanyi Dong, Yan Yan, Wei Bian, and Yi Yang. Progressive learning for person re-identification with one example. *IEEE Transactions on Image Processing*, 28(6):2872–2881, 2019.
- [37] Bryan Ning Xia, Yuan Gong, Yizhe Zhang, and Christian Poellabauer. Second-order non-local attention networks for person re-identification. In *Proceedings of the IEEE International Conference on Computer Vision*, pages 3760–3769, 2019.
- [38] Kelvin Xu, Jimmy Ba, Ryan Kiros, Kyunghyun Cho, Aaron Courville, Ruslan Salakhudinov, Rich Zemel, and Yoshua Bengio. Show, attend and tell: Neural image caption generation with visual attention. In *International Conference on Machine Learning*, pages 2048–2057. PMLR, 2015.
- [39] Mang Ye, Xiangyuan Lan, Qingming Leng, and Jianbing Shen. Cross-modality person re-identification via modality-aware collaborative ensemble learning. *IEEE Transactions on Image Processing*, 29:9387–9399, 2020.
- [40] Mang Ye, Xiangyuan Lan, Jiawei Li, and Pong Yuen. Hierarchical discriminative learning for visible thermal person re-identification. In *Proceedings of the AAAI Conference on Artificial Intelligence*, volume 32, 2018.
- [41] Mang Ye, Xiangyuan Lan, Zheng Wang, and Pong C Yuen. Bi-directional center-constrained top-ranking for visible thermal person re-identification. *IEEE Transactions on Information Forensics and Security*, 15:407–419, 2019.
- [42] Mang Ye, Jianbing Shen, David J. Crandall, Ling Shao, and Jiebo Luo. Dynamic dual-attentive aggregation learning for visible-infrared person re-identification. In *European Conference on Computer Vision*, 2020.
- [43] Mang Ye, Zheng Wang, Xiangyuan Lan, and Pong C Yuen. Visible thermal person re-identification via dual-constrained top-ranking. In *Proceedings of International Joint Conference on Artificial Intelligence*, volume 1, page 2, 2018.
- [44] Sergey Zagoruyko and Nikos Komodakis. Paying more attention to attention: Improving the performance of convolutional neural networks via attention transfer. *arXiv preprint arXiv:1612.03928*, 2016.
- [45] Xiaolin Zhang, Yunchao Wei, Guoliang Kang, Yi Yang, and Thomas Huang. Self-produced guidance for weakly-supervised object localization. In *Proceedings of the European Conference on Computer Vision*, pages 597–613, 2018.
- [46] Liang Zheng, Yi Yang, and Alexander G Hauptmann. Person re-identification: Past, present and future. *arXiv preprint arXiv:1610.02984*, 2016.
- [47] Zhedong Zheng, Xiaodong Yang, Zhiding Yu, Liang Zheng, Yi Yang, and Jan Kautz. Joint discriminative and generative learning for person re-identification. In *Proceedings of the IEEE Conference on Computer Vision and Pattern Recognition*, pages 2138–2147, 2019.
- [48] Zhedong Zheng, Liang Zheng, and Yi Yang. A discriminatively learned cnn embedding for person reidentification. *ACM Transactions on Multimedia Computing, Communications, and Applications*, 14(1):1–20, 2017.
- [49] Zhedong Zheng, Liang Zheng, and Yi Yang. Unlabeled samples generated by gan improve the person re-identification baseline in vitro. In *Proceedings of the IEEE International Conference on Computer Vision*, pages 3754–3762, 2017.
- [50] Jun-Yan Zhu, Taesung Park, Phillip Isola, and Alexei A Efros. Unpaired image-to-image translation using cycle-consistent adversarial networks. In *Proceedings of the IEEE International Conference on Computer Vision*, pages 2223–2232, 2017.